Characterization and Dissolution Studies of a Benzophenone-Containing Organic-Soluble Polyimide

Hurng-Rern Lee, Tsai-An Yu, and Yu-Der Lee*

National Tsing Hua University, Department of Chemical Engineering, Hsinchu, Taiwan, ROC 30043. *Received March 16, 1989; Revised Manuscript Received June 16, 1989*

ABSTRACT: An organic soluble benzophenone-containing polyimide (BCPI) was synthesized via solution polycondensation of 3,3',4,4'-benzophenonetetracarboxylic dianhydride with 2,3,5,6-tetramethyl-*p*-phenylenediamine. The dissolution characteristics were studied by using a dissolution apparatus. Experimental data showed that the normalized thickness of the gel layer (δ), the position of the rubbery/solvent interface S, and the position of the rubbery/glassy interface R were linear and proportional to the square root of the diffusion time at an early stage of dissolution process. As experimental time proceeded, dissolution became more apparent and the linear relationship would no longer exist. Mathematical models to describe the dissolution behavior of BCPI in *N*-methyl-2-pyrrolidone (NMP) were proposed. Discrepancies between experimental data and theoretical values were within an acceptable range. Activation energies of the diffusion coefficient (D_1) and the dissolution/mass transfer coefficient (k) were found to be 1.2 and 1.84 kcal/mol, respectively. Effects of the diffusion coefficient (D_1), the difference between polymer volume fractions at two interfaces ($c^* - c_d$), and the dissolution/mass transfer coefficient (k) on the normalized thickness of the gel layer (δ) were also discussed.

Introduction

Polyimide is used in the manufacture of integrated circuits for passivation coatings, interlayer dielectrics, α-particle barriers, and insulating layers in a variety of other applications. Because of their insolubility, combined with their high glass transition temperatures, they are difficult to fabricate. In fact, most polyimides are processed in the form of their poly(amic acid) precursors, which are then thermally or chemically converted to the imide structure. Harris et al.[1] had found that several thermally stable polyimides were soluble in organic solvents. Recently, reports of an organic-soluble photosensitive polyimide appeared in the literature. Pfeifer and Rhode[2] discovered that fully imidized organic-soluble polyimides carrying the following structural unit

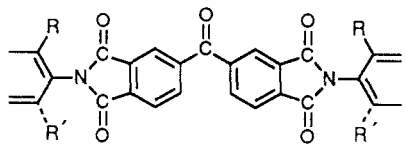

were intrinsically photosensitive when R stands for an aliphatic group and R' represents an optional aliphatic substituent, which may or may not be identical with R. Lin and co-workers,[3] on the other hand, studied the crosslinking mechanism of these polyimide systems. Nakano[4] developed photosensitive and nonphotosensitive polyimides that were soluble in *N*-methyl-2-pyrrolidone (NMP). These organic-soluble polyimides had been prepared from biphenyltetracarboxylic dianhydride and various aromatic diamine compounds. Photosensitive polyimide becomes attractive because it provides both insulative and photoresist functions; consequently the number of steps can be reduced in the process of image formation. The formation of these images in a film can be accomplished by the use of particular exposure patterns and then selective dissolution of the exposed or unexposed regions according to positive- or negative-type photoresists. One of the important characteristics of candidate materials for these applications is their dissoluiton behavior in organic solvents. The process of dissolution is rather complex. At an early stage of the solvent contacting the glassy polymer, the solvent molecules interact thermodynamically with the macromolecular chains according to the principles of the Flory-Huggins theory.[5] Thus, individual chains change from their unperturbed state to a new solvated state. Their end-to-end distance increases by an expansion factor that depends on the polymer/solvent Flory interaction parameter χ or on their respective solubility parameters δ_p and δ_s. The transport mechanism may be Fickian or non-Fickian during the early stage of solvent transport. However, the solvent-transport mechanism becomes purely Fickian in samples of thicknesses greater than a few micrometers. Beyond the swelling stage, the macromolecular chains pass through a region where the high solvent concentration leads to dissolution.[6] The solvent dissolution process of a polymer slab is shown in Figure 1. Two different fronts are formed at the solvent/glassy interface as soon as solvent contacts with polymer. During the swelling stage (Figure 1b), a rubbery/glassy interface R moves inward and a rubbery/solvent interface S moves outward gradually. The movements of interfaces R and S are due to volume expansion. During the dissolution step (Figure 1c), the front R continues to move inward. In the meantime, the front S continues to move outwardly but the expansion rate is slower than that during the initial swelling step. The cause is that the effect of dissolution becomes important. In the next step (Figure 1d) the front R continues to move inward until two symmetrical fronts meet in the center of the film, i.e., the polymer is totally swollen, and front S starts moving inward because dissolution becomes more evident. After fronts R at both sides of the slab have met in the center of the film, only front S remains for the diffusion/dissolution process (Figure 1). The front S continues to move inward until all of the polymer sample has been dissolved.

Studies on dissolution phenomena of glassy polymers have appeared in the literature only occasionally. Ueberreiter and Asmussen[7,8] gave a description of an apparatus for measuring the dissolution behavior of a polymer and the mathematical treatment of dissolution data. They also suggested that the dependences of the thickness of

* To whom correspondence should be addressed.

0024-9297/90/2223-0502$02.50/0

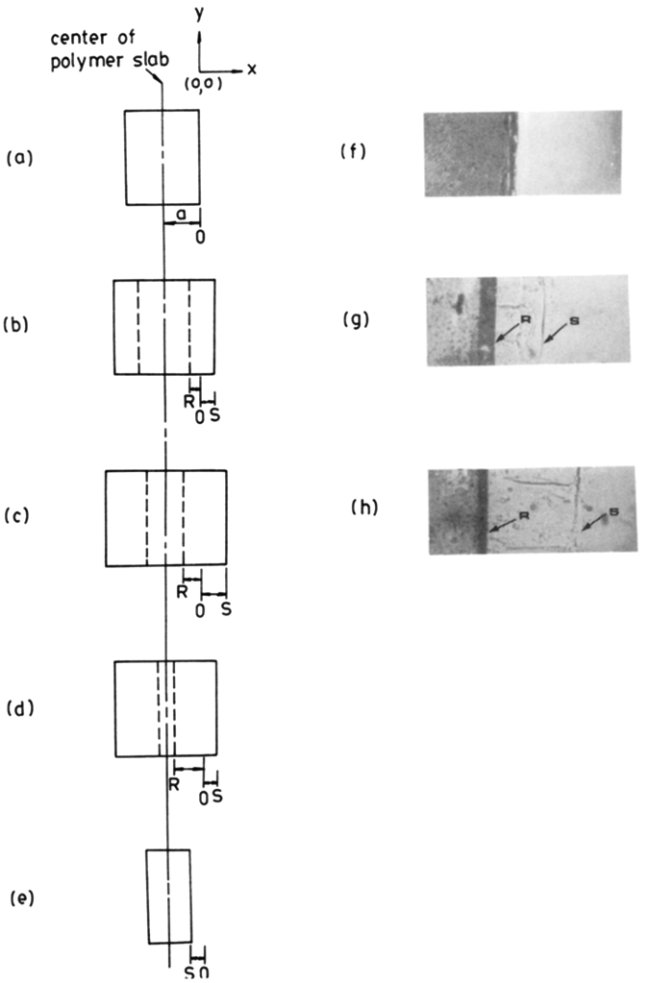

Figure 1. Schematic representation of the dissolution phenomenon of a polymer slab: (a) initial slab thickness $2a$; (b) initial swelling step showing the increasing position of the rubbery/solvent interface S and the decreasing position of the rubbery/glassy interface R; (c) continuous swelling and beginning of dissolution step showing that interface S moves outward slower than step b and interface R moves inward continuously; (d) dissolution step showing that interfaces R and S move inward; (e) final dissolution step showing that interfaces R at two sides of the slab have met in the center of the polymer slab and interface S moves inward continuously; photomicrographs of BCPI in NMP at 51.0 °C; (f) experimental observation for t = 0 min; (g) experimental observation for t = 12.5 min; (h) experimental observation for t = 113 min.

a swollen gel layer and the dissolution rate on temperature were exponential functions. Ouano and Carothers[9,10] studied the dissolution rate of irradiated PMMA and found that the increase in the dissolution rate of irradiated PMMA could be attributed to the reduction in the molecular weight and the formation of nonpolymeric volatile fragments by radiation exposure as well as the increase in the "excess free volume" due to the volatilization of low molecular weight fragments. Cooper et al.[11] used a laser interferometer to measure in situ the dissolution rates of thin films of PMMA and found that solvent mixtures containing small amounts of a low molecular weight nonsolvent and a higher molecular weight good solvent had an increased dissolution rate. Parsonage and Peppas[12] also studied the dissolution characteristics of irradiated PMMA and poly(methyl methacrylate-*co*-maleic anhydride). Greeneich[13,14] had studied the developer characteristics and solubility rate of PMMA. Soane et al.[15] used a single-element rotating-polarizer ellipsometer (psi meter) to study the influence of processing and the molecular parameter on the dissolution rate of a PMMA thin film (<1 μm) in methyl isobutyl ketone.

Recent interest in photoresist development leads to a need to reexamine the polymer dissolution kinetics. However, mathematical modeling of the polymer dissolution process has not been undertaken except for the works of Ueberreiter and Asmussen,[7] Tu and Ouano,[16,17] and Parsonage[12] et al. In our previous work,[18] a benzophenone-containing polyimide (BCPI) with structural unit

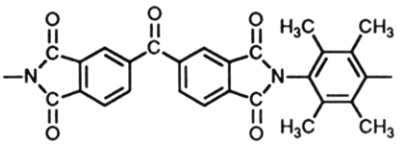

was found to be organic soluble. In this paper, we continued to study the dissolution process of BCPI in NMP in detail. In addition to temperature effects, mathematical models that can effectively analyze the data at the early stage of our dissolution process were also proposed.

Experimental Section

Materials. 3,3′,4,4′-Benzophenonetetracarboxylic dianhydride (BTDA) (Polyscience) was recrystallized from acetic anhydride and dried under reduced pressure at 200 °C before use. 2,3,5,6-Tetramethyl-*p*-phenylenediamine (TMPD) (Fluka) was recrystallized from alcohol and dried under reduced pressure. *N*-Methyl-2-pyrrolidone (NMP) (Merck) was distilled before being stored in 4-Å molecular sieves.

Preparation and Characterization of Polyimide. TMPD, dissolved in NMP at room temperature, was taken in a reaction flask fitted with a nitrogen purge system. The solution was cooled to 0 °C when equivalent moles of BTDA were added to the solution with stirring. Afterward, the temperature of the solution with 20% solid content was raised to room temperature and allowed to react for 24 h. Thus, poly(amic acid) was obtained. Chemical imidazation was carried out by treating the poly(amic acid) in NMP with a mixed solvent of acetic anhydride and pyridine (mole ratio of acetic anhydride:pyridine = 4:3.5 mol per mol of poly(amid acid)[19] at 60 °C for 8 h. The final solution was added to methanol dropwise so as to allow the polyimide to precipitate. The intrinsic viscosity run at a concentration of 5 g/dL in NMP at 30 °C was 1.04 dL/g. The powder form of polyimide was transformed into films by the following procedures. A concentrated solution (20 wt % polyimide in NMP) was first cast at room temperature on a cleaned glass plate and then placed in a forced-ventilation oven at 80 °C for 30 min, 100 °C for 30 min, and finally 200 °C for 2 h to allow gentle and complete evaporation of the solvent. The above procedures were repeated so as to obtain a desirable final thickness. After cooling to room temperature, these films were extracted with water overnight in a Soxhlet apparatus, vacuum dried, and cut into slabs for dissolution studies. The dimensions of the polyimide slabs were 40 × 2 × 0.2 mm^3.

Infrared spectra of the poly(amic acid) and polyimide were taken by using a Perkin-Elmer 842 IR spectrophotometer and are given in Figure 3. In spectrum a, which corresponds to poly(amic acid), the absorption band in the range of 3100–3300 cm^{-1} is due to the stretching of O–H, and the absorption band at 1660 cm^{-1} is due to secondary amide groups. In spectrum b, which represents BCPI structure, the absorption bands at 1780 and 1730 cm^{-1} are related to symmetrical and asymmetrical stretching of C=O of imide group, respectively, while the absorption bands at 1100 and 720 cm^{-1} are the vibrations of the imide structure.

NMR spectrum was run by Bruker AM-400 and given in Figure 4. The NMR spectrum is in agreement with the proposed structure. BCPI shows a singlet at 2.08 ppm for the protons of the methyl groups and a doublet, centered at 8.35 ppm (J = 8.0 Hz), a singlet at 8.31 ppm, and a doublet, centered at 8.26 ppm (J = 8.0 Hz), for the protons on the benzene ring.

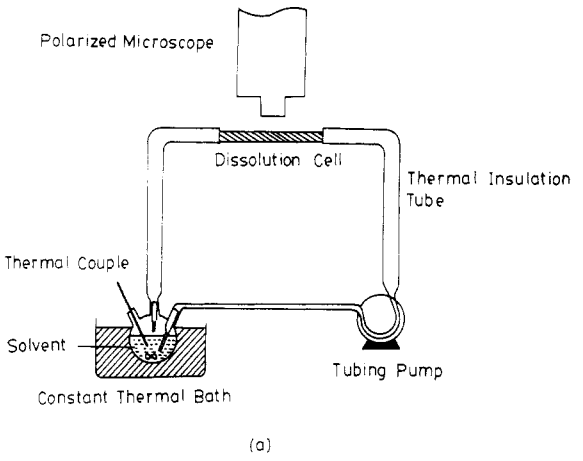

Figure 2. Schematic apparatus for dissolution measurements: (a) the whole set up; (b) interior of the dissolution cell viewed from the top.

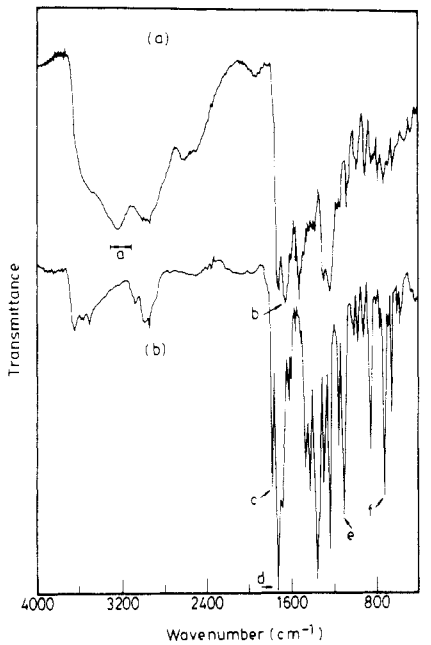

Figure 3. Infrared spectra of poly(amic acid) and BCPI: (a) polyamic acid; (b) BCPI. a, 3100–3300 cm^{-1}; b, 1660 cm^{-1}; c, 1780 cm^{-1}; d, 1730 cm^{-1}; e, 1100 cm^{-1}; f, 720 cm^{-1}.

The density of BCPI was measured by a pycnometric method and determined to be 1.35 g/cm^3. The determinations of glass transition temperature and TGA curve were made by a SEIKO I SSC-5000 thermal analyzer with a heating rate of 10 °C/min in N_2.

Measurements of Dissolution. Measurements of dissolution were performed in NMP at 20–60 °C by using a polarized microscope and the dissolution apparatus shown in Figure 2. The dissolution cell was composed of two glass slices and two glass strips with thicknesses of 18 μm. The glass strips were set between the slices along the edges so as to form a cell with constant spacing between the slices. Epoxy resin was used to seal the edges to avoid leakage. A sample film was put inside the cell before sealing. Since the thickness of the sample film (around 20 μm) was larger than that of the glass strip (18 μm), the sample film was supported in the cell by compression. The flow rate of solvent was set to be 1 cm^3/min. The positions of the rubbery/glassy interface R and rubbery/solvent interface S could be viewed on a microscope and pictured at various experimental time. Thus, interfaces R and S could be measured independent if the original position at $t = 0$ was fixed.

The diffusion coefficients of BCPI in NMP at various temperatures were measured by using a DLS-700 light scattering apparatus (Japan Otsuka Electric Co.)[20-24] at the concentration of 0.01 g/mL in NMP.

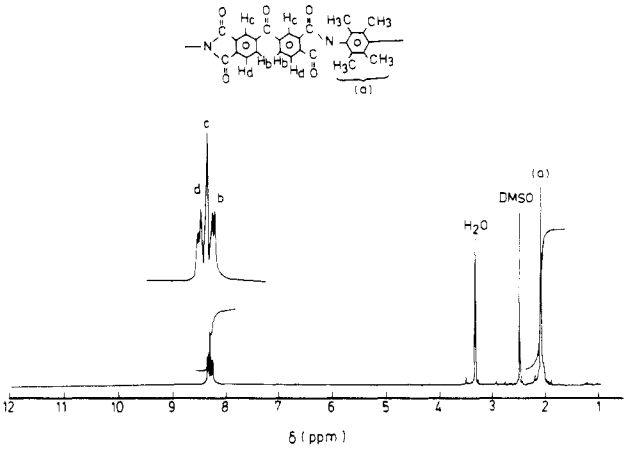

Figure 4. ^1H NMR spectrum of BCPI in DMSO-d_6.

Table I
Characteristics of BCPI

T_g[a]	421.1°C
density	1.35 g/cm^3
M_w[b]	4.2×10^4
intrinsic viscosity[c]	1.04 dL/g
good solvents	*m*-cresol
	N,N-dimethylacetamide
	N,N-dimethylformamide
	hexamethylphosphoramide
	N-methyl-2-pyrrolidone
	tetramethylurea

[a] Value in the literature[2] is 439 °C. [b] Measured on a light scattering apparatus. [c] Measured in NMP at 30 °C.

Results and Discussion

Characteristics of BCPI. Characteristic properties of BCPI are listed in Table I. It was found that good solvents for BCPI were mostly amides. The three-dimensional solubility parameters of BCPI were found to be $\delta_{d,p} = 10.6$ $cal^{1/2}$ $cm^{-3/2}$, $\delta_{p,p} = 5.3$ $cal^{1/2}$ $cm^{-3/2}$, $\delta_{h,p} = 5.3$ $cal^{1/2}$ $cm^{-3/2}$, while the total solubility parameter δ_p was 12.98 $cal^{1/2}$ $cm^{-3/2}$.[18]

On inspection of spectra a and b in Figure 3, the disappearance of absorption bands at 3100–3300 and 1660 cm^{-1} and the appearance of absorption bands at 1780, 1730, 1100, and 720 cm^{-1} indicate a rather complete imidization. The imide structure can be further proven by NMR spectroscopy. Figure 4 shows the NMR spectrum of BCPI in dimethyl-d_6 sulfoxide (DMSO-d_6). No characteristic peaks of a carboxylic group (>10 ppm) were observed. The thermal stability of BCPI was evaluated from the thermogravimetric curve shown in Figure 5. The initial decomposition temperature was 300 °C, at which the methyl groups of BCPI started to dissociate. The

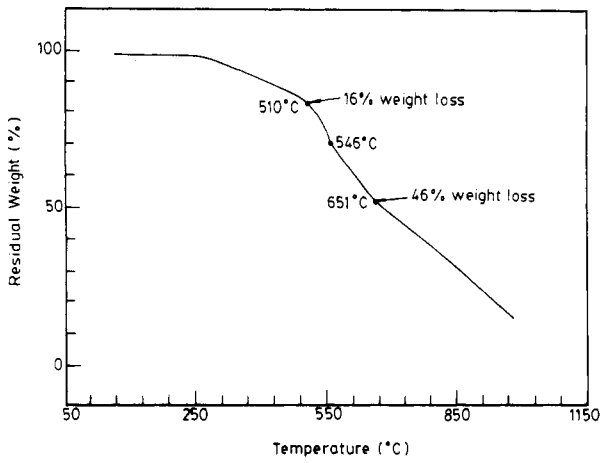

Figure 5. Thermogravimetric curve of BCPI. Heating rate = 10 °C/min in N_2.

16% weight loss of BCPI at 510 °C is considered to be the decomposition of methyl groups of BCPI, the theoretical value of which is 12% weight loss. The maximum decomposition temperature occurs at 546 °C, at which a primary scission process occurs at the imide bonds (C—N), followed by second cleavage (C—C) resulting in the elimination of C=O groups.[25] The 46% weight loss of BCPI at 651 °C is thought to be the decomposition of imide structures and ketone groups of BCPI, the theoretical value of which is 35% weight loss.

Simplified Model for Dissolution. Before analyzing the experimental data of BCPI dissolved in NMP, a model to describe the swelling and dissolution phenomenon of a polymer was developed. Three assumptions were made during derivation of the model. The first is that the volume-based polymer diffusion coefficient (D_1) is independent of concentration. The second is that the value of D_1 at interface R is the same as D_1 at interface S. The third is the assumption of a pseudo-steady-state condition; i.e., the time-dependent term of eq 1 can be neglected. The Fickian diffusion equation shown in eq 1 characterizes the solvent transport into a thin polymer slab (Figure 1), where D_1 is the volume-based polymer

$$\frac{\partial c_2}{\partial t} = \frac{\partial}{\partial x}\left(D_1\frac{\partial c_2}{\partial x}\right) = D_1\frac{\partial^2 c_2}{\partial^2 x} \tag{1}$$

diffusion coefficient in the solvent, c_2 is the polymer volume fraction, x is position, and t is diffusion time. Because the movements of solvent and polymer are simultaneous, the volume fractions of solvent and polymer are expressed as c_1 and c_2, respectively. Thus

$$c_1 + c_2 = 1 \tag{2}$$

Equation 1 can be solved by the following set of initial and boundary conditions described by eq 3–7.

At the initial time of the experiment, the rubbery/glassy interface R and solvent/rubbery interface S are at the same position, which is set to be the origin, i.e.

$$t = 0, \quad R = S = 0 \tag{3}$$

The interfaces R and S separate as soon as the experiment starts. The polymer volume fraction c^* at the interface R is controlled only by the thermodynamic characteristics of the transport problem, which can be calculated and will be shown later. Thus

$$t > 0, \quad -a < x = R < 0, \quad c_2 = c^* \tag{4}$$

where a is half the original thickness of the BCPI sample, i.e., $2a$ = 0.2 cm in our experimental conditions.

When the interface R moves toward the center of the slab, the solvent passes through the interface R due to the volume expansion of the slab, i.e.

$$t > 0, \quad -a < x = R < 0, \quad D_1\frac{\partial c_2}{\partial x} = (1 - c_2)\frac{\partial R}{\partial t} \tag{5}$$

During the experiment, the interface S is assumed to have a polymer volume fraction c_d, at which the macromolecular chains begin to disentangle and start to dissolve, i.e.

$$t > 0, \quad x = S > 0, \quad c_2 = c_d \tag{6}$$

Finally, the movement of interface S is the result of both penetrant transport and polymer dissolution. Thus

$$t > 0, \quad x = S > 0, \quad -D_1\frac{\partial c_2}{\partial x} - kc_d = (1 - c_2)\frac{\partial S}{\partial t} \tag{7}$$

where k is the dissolution/mass transfer coefficient and c_d is the polymer volume fraction at interface S. The exact solution of eq 1 is rather cumbersome and required a more detailed analysis, which will be shown later. However, a simpler solution can be obtained by assuming the pseudo-steady-state condition; i.e., the solution may be solved by neglecting the time-dependent term of eq 1. Thus, eq 5 and 7 can be transformed to eq 8 and 9, respectively:

$$(1 - c^*)\frac{dR}{dt} = \frac{D_1(1 - c_d)}{S - R} \tag{8}$$

where c^* is the polymer volume fraction at interface R and

$$(1 - c_d)\frac{dS}{dt} = \frac{D_1(c^* - c_d)}{S - R} \tag{9}$$

To solve the problem, a normalized thickness of the gel layer is introduced, according to

$$\delta = (S - R)/a \tag{10}$$

Then, eq 8 and 9 can be solved to give

$$\frac{t}{a^2} = -\frac{(1 - c_d)\delta}{akc_d} - \frac{D_1(1 - c_d)^2(c^* - c_d)}{(akc_d)^2}\left(\frac{1}{1 - c_d} + \frac{1}{1 - c^*}\right) \times \ln\left[1 - akc_d/\left[D_1(c^* - c_d)(1 - c_d)\left(\frac{1}{1 - c_d} + \frac{1}{1 - c^*}\right)\right]\right] \tag{11}$$

The logarithmic function of the second term on the right side of eq 11 can be expanded into a polynomial and only the first- and second-order terms are kept. The final result is

$$\delta = \left[\frac{2D_1(c^* - c_d)}{a^2}\left(\frac{1}{1 - c_d} + \frac{1}{1 - c^*}\right)t\right]^{1/2} \tag{12}$$

Equations 12 and 10 are substituted into eq 8. The interface R at any time can be calculated and is given as

$$R = -\left[\frac{2D_1(c^* - c_d)t}{(1 - c^*)^2\left(\frac{1}{1 - c_d} + \frac{1}{1 - c^*}\right)}\right]^{1/2} \tag{13}$$

The approximate pseudo-steady-state solution suggests that the normalized gel layer thickness δ and interface R increase linearly with respect to $t^{1/2}$ at the early stage of the dissolution process. Because eq 12 is independent of k, the influence of dissolution can be neglected at an early stage of the dissolution process. Therefore the second term of the right side of eq 9 may be omitted. Thus, the position of interface S at an early stage

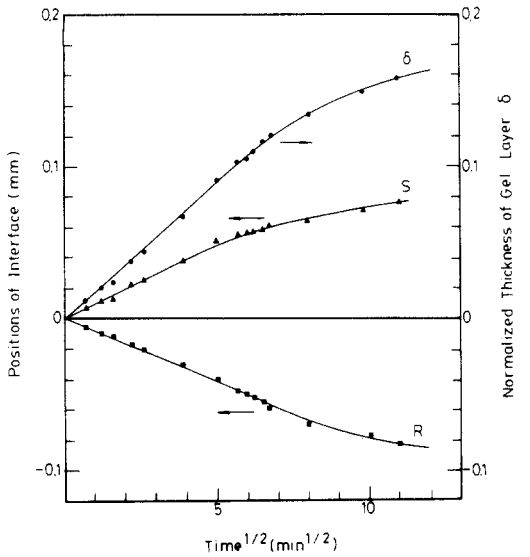

Figure 6. Normalized gel layer thickness δ (●), position of the rubbery/solvent interface S (▲), and position of the rubbery/glassy interface R (■) plotted against the square root of time. Temperature = 27.8 °C.

of the dissolution process can be described by

$$S = \left[\frac{2D_1(c^* - c_d)t}{(1-c_d)^2\left(\frac{1}{1-c_d} + \frac{1}{1-c^*}\right)}\right]^{1/2} \tag{14}$$

The position of interface S also increases linearly with respect to $t^{1/2}$ at an early stage of the dissolution process just as the literature has described.[17]

Experimental Dissolution Results. Dissolution studies of BCPI were performed in NMP at various temperatures. In general, the dissolution process was expected to start with the formation of a thin gel layer and to be accompanied by considerable swelling. Indeed, two fronts were observed as shown in Figure 1g,h; front S separates the solvent from the rubbery-like material, and front R separates the rubbery-like material from the glassy polymer. During the experiment, the solvent transported into the glassy polymer until the volume fraction of solvent at the interface became large enough to disentangle the glassy polymer. In other words, as the polymer volume fraction at the interface reached c^*, two fronts began to separate. The thickness of gel layer increased due to the transportation of the solvent, which totally disentangled the swollen macromolecular chains. At this point, true dissolution was observed. Beyond this point, the dissolution rate was faster than the swelling rate. Therefore, although the interface R receded, the gel layer thickness decreased. One set of dissolution data containing the normalized gel layer thickness (δ), the rubbery/glassy interface R, and the solvent/rubbery interface S are plotted as a function of the square root of time in Figure 6. There is a linear increase of each thickness or position (δ, R, S) with respect to $t^{1/2}$ at the early stage of the dissolution process. Figures 7 and 8 show the temperature effect on the normalized thickness of the gel layer and positions of two interfaces, respectively. As expected, higher temperatures result in faster swelling and dissolution rate. Figures 7 and 8 also illustrate that the normalized thickness of the gel layer (δ), interface R, and interface S increase with $t^{1/2}$ linearly at an early stage of the dissolution process. However, at the latter stage of the dissolution process, the linear relationship between the normalized thickness of the gel layer (δ), interface R, or interface S with $t^{1/2}$ does not exist anymore. This is because the effect

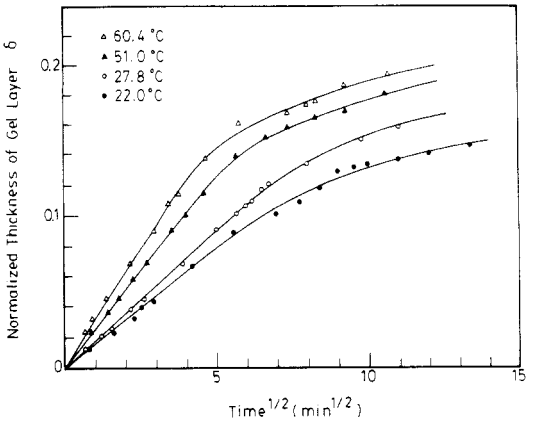

Figure 7. Normalized thickness of gel layer plotted against the square root of time at various temperatures.

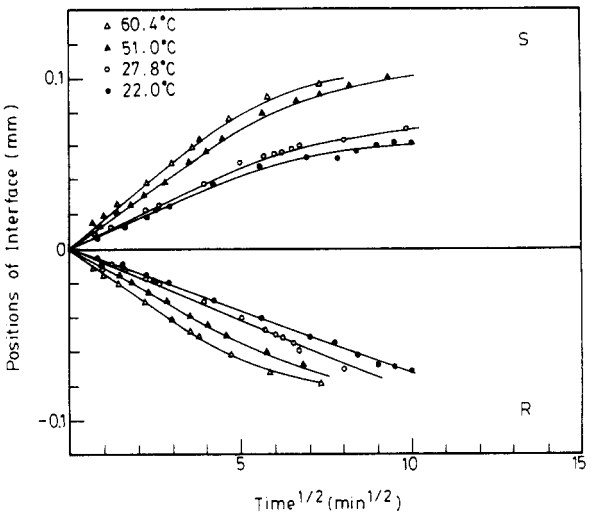

Figure 8. Positions of the interfaces R and S plotted against the square root of time at various temperatures.

of dissolution can no longer be neglected at this stage. Clearly, the simplified model is valid at the initial stage but inadequate to describe the whole dissolution process.

Determinations of Polymer Volume Fractions at Two Interfaces and Dissolution/Mass Transfer Coefficients at Various Temperatures. In order to analyze further the dissolution process, two important parameters need to be determined beforehand. One is the value of critical solvent concentration for a polymer transition from the glass state to the rubbery state, c^*_0, and it is determined according to[26]

$$c^*_0 = \frac{T_b - T}{(\beta/\alpha_f)} \tag{15}$$

where T_g is the value of the glass transition temperature of BCPI and T is the experimental temperature. The linear expansion coefficient is estimated by[27]

$$\alpha_f = \frac{B_1}{2.303 c_0^1 c_0^2} \tag{16}$$

where B_1 has usually been set arbitrarily equal to unity, while c_0^1 and c_0^2 are estimated to be 17.44 and 51.6, respectively. β is a parameter representing the contribution of the given diluent to the increase of free volume. Fujita and Kishimoto[26] yielded values of β within the range 0.08–0.3 for different polymers. Here, the value of β is taken to be 0.2. From these values, c^*_0 (*grams* of solvent/gram of polymer) was calculated and then transformed

Table II
Values of c^*, D_1, c_d, and k at Various Temperatures

temp, °C	c^{*a}	$10^7 D_1$, cm²/s[b]	c_d[c]	$10^6 k$, cm/s[d]
22.0	0.44	1.5	0.402	0.95
27.8	0.45	2.1	0.407	1.05
51.0	0.46	3.5	0.418	2.90
60.4	0.46	4.5	0.415	4.00

[a] Polymer volume fraction at interface R. [b] Diffusion coefficient measured by the dynamic light scattering method. [c] Polymer volume fraction at interface S. [d] Dissolution/mass transfer coefficient.

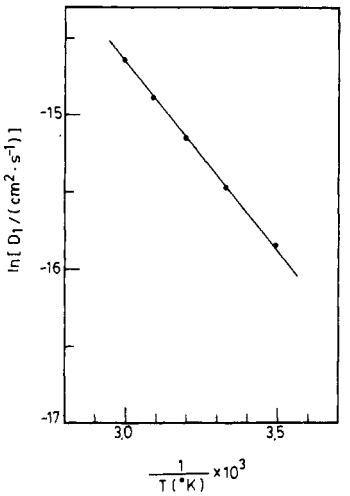

Figure 9. Logarithmic diffusion coefficients (D_1) versus reciprocal temperatures.

to the polymer volume fraction c^* according to

$$c^* = \frac{1}{\rho_p}\left(\frac{c^*_0}{\rho_p} + \frac{1}{\rho_s}\right)^{-1} \tag{17}$$

where ρ_p and ρ_s are the densities of dry BCPI and NMP, respectively (ρ_s = 1.03 g/cm³). The other parameter is the value of the diffusion coefficient, which can be measured by a dynamic light scattering method.[20-24] The values of c^* and D_1 at various temperatures are listed in Table II. Since the T_g of BCPI is very high (421.1 °C), the changes of c^* with experimental temperatures are not significant; nevertheless, an increase of c^* with rising temperature is observed. The plot of logarithmic D_1 versus reciprocal temperature is shown in Figure 9, from which the activation energy is calculated to be 1.2 kcal/mol.

Generalized Model for Dissolution. The pseudo-steady-state solution has been solved and is given in eq 11. The solution of eq 1 without making the pseudo-steady-state assumption will be given here. Before solving the problem, the following dimensionless variables are defined

$$t' = t/(a^2/D_1) \tag{18}$$

$$x' = x/a \tag{19}$$

$$c = (c_2 - c^*)/(c_d - c^*) \tag{20}$$

$$R' = R/a \tag{21}$$

$$S' = S/a \tag{22}$$

Then, substituting eq 18–20 into eq 1 gives

$$\partial c/\partial t' = \partial^2 c/\partial x'^2 \tag{23}$$

From the dimensionless variables, the initial and boundary conditions of eq 3–7 become

$$t' = 0, \quad R' = S' = 0 \tag{24}$$

$$t' > 0, \quad x' = R', \quad c = 0 \tag{25}$$

$$t' > 0, \quad x' = R', \quad \frac{\partial R'}{\partial r'} = A\left(\frac{\partial c}{\partial c'}\right) \tag{26}$$

$$t' > 0, \quad x' = S', \quad c = 1 \tag{27}$$

$$t' > 0, \quad x' = S', \quad \frac{\partial S'}{\partial t'} = -B\left(\frac{\partial c}{\partial x'}\right) - E \tag{28}$$

where

$$A = (c_d - c^*)/(1 - c^*) \tag{29}$$

$$B = (c_d - c^*)/(1 - c_d) \tag{30}$$

$$E = (akc_d)/[(1 - c_d)D_1] \tag{31}$$

Here the origin is set at the center of the polymer slab for a more convenient calculation. By subtraction of eq 28 from eq 26, it follows that

$$\frac{\partial \delta}{\partial t'} = -B\frac{\partial c}{\partial x'}\bigg|_{x'=S'} - EA\frac{\partial c}{\partial c'}\bigg|_{x'=R'} \tag{32}$$

Equation 23 can be solved by the separation of variables method, and the final solution of eq 23 is

$$c = \sum_{n=-\infty}^{\infty} \frac{2}{n\pi}(-1)^n \sin(\lambda_n \bar{x}) e^{-\lambda_n^2 t} \frac{\bar{x}}{\delta} \tag{33}$$

where $\bar{x} = x' - R'$ and $\lambda_n = n\pi/\delta$. Differentiating the concentration distribution in eq 33 with respect to x' and taking the values of $x' = R'$ and $x' = S'$ respectively give

$$\frac{\partial c}{\partial x'}\bigg|_{x'=R'} = \frac{1}{\delta}\left[\sum_{n=-\infty}^{\infty} 2(-1)^n e^{-\lambda_n^2 t} + 1\right] \tag{34}$$

$$\frac{\partial c}{\partial x'}\bigg|_{x'=S'} = \frac{1}{\delta}\left[\sum_{n=-\infty}^{\infty} 2e^{-\lambda_n^2 t} + 1\right] \tag{35}$$

Equations 34 and 35 can also be used to obtain R' and S' by employing the Runge–Kutta method.

Substituting eq 34 and 35 into eq 32 gives

$$\frac{1}{2}\frac{d\delta^2}{dt} = \sum_{n=-\infty}^{\infty} -2[B + (-1)^n A]e^{-\lambda_n^2 t} - (A + B) - E\delta \tag{36}$$

Because eq 36 is a kind of first-order time-dependent nonlinear ordinary differential equation, numerical analysis by the Runge–Kutta fourth-order method is used to calculated the normalized thickness of the gel layer (δ) as a function of time with the initial condition $t = 0$, $\delta = 0$.

The right side of eq 36 has three terms: the first term is the transition state term; the second term is the steady-state term; and the third term is the dissolution term. The order of magnitude of the second term is larger than those of the first and third terms at small t. Therefore, the first and third terms can be neglected at the early stage of the dissolution process. Thus, the solution of eq 36 with only the steady-state term remaining is the same as eq 11, which we have developed previously. As the experimental time proceeds, the third term can no longer be neglected and becomes more and more important for the normalized thickness of the gel layer.

Experimental determination of the value of c_d, the polymer volume fraction at which the polymer begins to disentangle and starts to dissolve, is appropriate here. From eq 36, c_d can be determined from Figure 6 at the initial time of the experiments. The values of c_d thus obtained are listed in Table II. It is seen that c_d is not very sensitive to temperature. Nevertheless, a higher temperature results in a higher c_d. The dissolution/mass transfer coefficient (k) can also be obtained by fitting eq 36

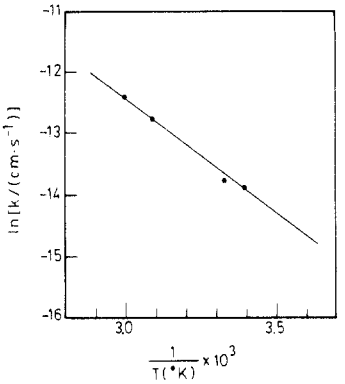

Figure 10. Logarithmic dissolution/mass transfer coefficients (k) versus reciprocal temperatures.

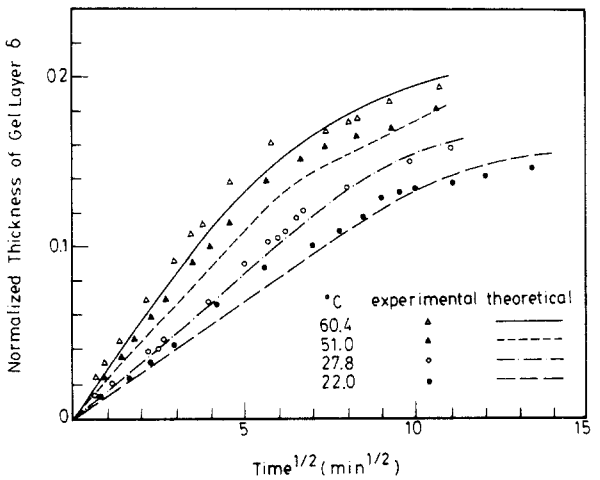

Figure 11. Comparison of the normalized thickness of the gel layer (δ) between experimental data and theoretical values at various temperatures. Points are experimental data and lines represent theoretical results.

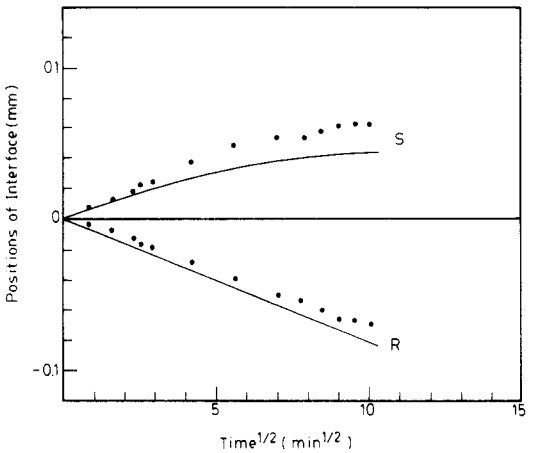

Figure 12. Comparisons between experimental data and theoretical values of interfaces R and S at 22.0 °C. Points are experimental data and lines represent the theoretical results.

with experimental data and the results are listed in Table II. The plot of logarithmic k versus reciprocal temperatures is shown in Figure 10, from which the activation energy is found to be 1.84 kcal/mol.

Comparisons between experimental data and theoretical values obtained by eq 36 are shown in Figure 11. Reasonable agreements are observed. Figure 12 shows the values of interfaces R and S measured experimentally and calculated from eq 34 and 35, respectively. Deviations were probably caused by the assumptions that D_1

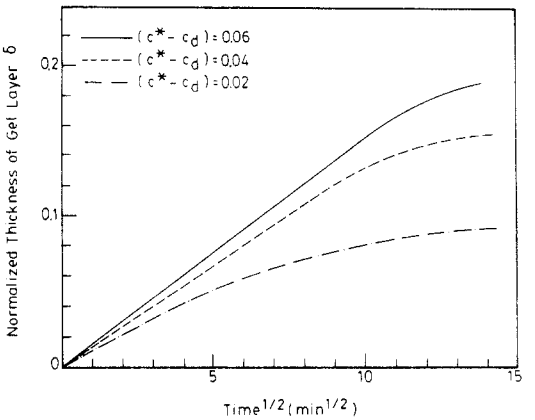

Figure 13. Effects of diffusion coefficients (D_1) on the normalized thickness of the gel layer (δ). Values of the polymer volume fraction at the interface $R(c^*)$, the polymer volume fraction at the interface $S(c_d)$, and dissolution/mass transfer coefficient (k) are 0.43, 0.392, and 9.5×10^{-7} cm/s, respectively.

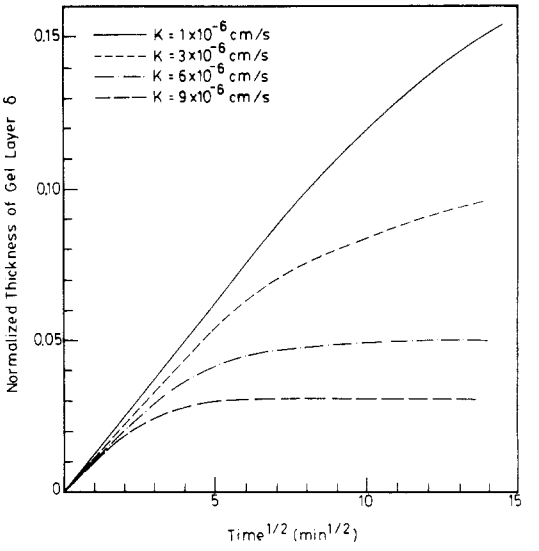

Figure 14. Effects of the difference of polymer volume fractions at two interfaces ($c^* - c_d$) on the normalized thickness of the gel layer (δ). c^* and c_d are polymer volume fractions at interfaces R and S, respectively. Values of the diffusion coefficient (D_1) and the dissolution/mass transfer coefficient (k) are 1.5×10^{-7} and 9.5×10^{-7} cm/s, respectively.

was constant and concentration independent at a preselected temperature.

By use of the model we have developed, the effects of the diffusion coefficient (D_1), the difference of polymer volume fractions at two interfaces ($c^* - c_d$), and the dissolution/mass transfer coefficient (k) on the normalized thickness of the gel layer (δ) are discussed by simulation. The normalized thickness of the gel layer (δ) versus the square root of time is plotted at various D_1 as shown in Figure 13. Higher D_1 results in larger δ because the flux of the polymer or solvent through the interface increases. The effect of ($c^* - c_d$) is shown in Figure 14. Larger ($c^* - c_d$) results in large flux and a higher value of δ. Different dissolution/mass transfer coefficients (k) also influence δ very much and the result is shown in Figure 15. Higher k causes a larger deviation in the linear relationship between δ and $t^{1/2}$. Physically, k represents the dissolution behavior. Higher k means a higher dissolution rate and dissolution occurs at a earlier during the process. As we have stated before, the linear relationship between δ and $t^{1/2}$ only exists at the early stage of the dissolution process, when true dissolution is negligible. This behavior can also be explained by statisti-

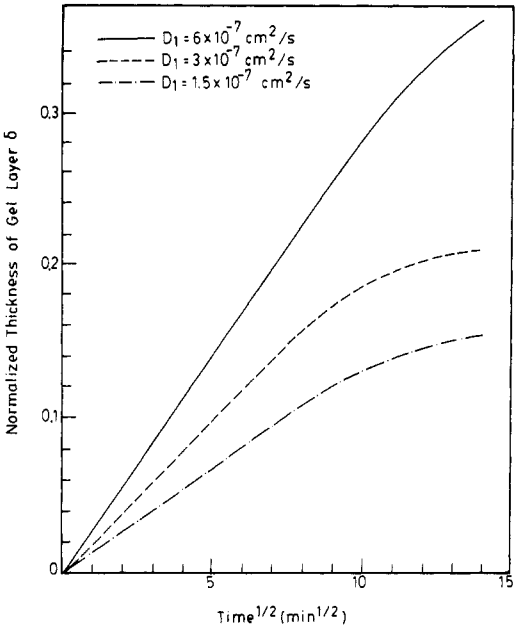

Figure 15. Effects of dissolution/mass transfer coefficients (k) on the normalized thickness of the gel layer (δ). Values of the polymer volume fraction at interface $R(c^*)$, the polymer volume fraction at the interface $S(c_d)$, and the diffusion coefficient (D_1) are 0.43, 0.392, and 1.5×10^{-7} cm²/s, respectively.

cal physics, which states the motion of the moment is a function of $t^{1/2}$;[28] i.e., if no dissolution occurs at interface S, the motion of macromolecules is a linear function of $t^{1/2}$. Once the effect of dissolution is obvious, the linear relationship of δ and $t^{1/2}$ will not exist.

Conclusions

The dissolution behavior of BCPI in NMP was studied in detail. It was found that the relationship between the normalized thickness of the gel layer (δ), the position of interface S, or the position of interface R and the square root of time was linear at an early stage of the dissolution process. However, these curves of δ, R, and S versus $t^{1/2}$ leveled off because dissolution/mass trans+fer effects became important as experimental time proceeded. Mathematical models with and without making pseudo-steady-state assumptions were presented. Models were supported by a series of experimental data. The concentrations at two interfaces R and S were not sensitive to temperature under our experimental conditions. The diffusion coefficient (D_1) and dissolution/mass transfer coefficient (k) were sensitive to temperature and had immense influence on dissolution characteristics. A larger diffusion coefficient, difference of polymer volume fractions at two interfaces ($c^* - c_d$), or dissolution/mass transfer coefficient resulted in a larger normalized thickness of the gel layer (δ). Finally, if the dissolution/mass transfer coefficient (k) was set equal to zero in the models, the normalized thickness of the gel layer (δ), the position of front S, and the position of front R would be linear with the square root of time. This was consistent with the experimental observation.

Acknowledgment. This research was sponsored by a grant from the National Research Council, Taiwan, ROC.

Registry No. (BTDA)(TMPD) (copolymer), 96211-25-5; (BTDA)(TMPD) (SRU), 96126-66-8; NMP, 872-50-4.

References and Notes

(1) Harris, F. W.; Feld, W. A.; Lanier, L. H. *ACS Polym. Prepr.* **1976**, *17*(2), 353.
(2) Pfeifer, J.; Rhode, O. *Proceedings of Second International Conference on Polyimides*; 1985, Oct 30–Nov 1; pp 130–150.
(3) Lin, A. A.; Sastri, V. R.; Jesoro, G.; Reiser, A.; Esachus, R. *Macromolecules* **1988**, *21*, 1165.
(4) Nakano, T. *Proceedings of Second International Conference on Polyimides*; 1985, Oct 30–Nov 1; pp 163–181.
(5) Flory, P. J. *Principles of Polymer Chemistry*; Cornell University Press: Ithaca, NY, 1953.
(6) de Gennes, P.-G. *Scaling Concept in Polymer Physics*; Cornell University Press: Ithaca, NY, 1979.
(7) Ueberreiter, K.; Asumussen, F. *J. Polym. Sci.* **1962**, *57*, 187.
(8) Asmussen, F.; Ueberreiter, K. *J. Polym. Sci.* **1962**, *57*, 199.
(9) Ouano, A. C. *Polym. Eng. Sci.* **1978**, *18*(4), 1160.
(10) Ouano, A. C.; Carothers, J. A. *Polym. Eng. Sci.* **1980**, *20*(2), 160.
(11) Cooper, W. J.; Krasicky, P. D.; Rodriguez, F. *J. Appl. Polym. Sci.* **1986**, *31*, 65.
(12) Parsonage, E. E.; Peppas, N. A.; Lee, P. I. *J. Vac. Sci. Technol.* **1987**, *B5*(2), 538.
(13) Greeneich, J. S. *J. Electrochem. Soc.* **1975**, *122*(7), 970.
(14) Greeneich, J. S. *J. Electrochem. Soc.* **1974**, *121*(12), 1669.
(15) Manjkow, J.; Papanu, J. S.; Hess, D. W.; Soane, D. S.; Bell, A. T. *J. Electrochem. Soc.* **1987**, *134*(8A), 2003.
(16) Tu, Y. O.; Ouano, A. C. *IBM J. Res. Develop.* **1977**, *21*, 131.
(17) Tu, Y. O. *Q. Appl. Math.* **1977**, *21*, 269.
(18) Lee, H. R.; Lee, Y. D. *J. Appl. Polym. Sci.*, in press.
(19) Vinogradova, S. V.; Vygodskii, Ya. S.; Vorobér, V. D.; Churochkina, N. A.; Chudina, L. I.; Spirina, T. N.; Korshak, V. V. *Polym. Sci. USSR* **1974**, *16*(3), 584.
(20) Reed, T. F.; Frederick, J. E. *Macromolecules* **1971**, *4*(1), 72.
(21) Kramer, O.; Frederick, J. E. *Macromolecules* **1972**, *5*(1), 69.
(22) Amis, E. J.; Janmey, P. A.; Ferry, J. D.; Yu, H. *Macromolecules* **1983**, *16*(3), 441.
(23) Hwang, D.-H.; Cohen, C. E. *Macromolecules* **1984**, *17*(9), 1679.
(24) Hwang, D.-H.; Cohen, C. E. *Macromolecules* **1984**, *17*(12), 2890.
(25) Heacock, J. F.; Berr, C. E. *Soc. Plast. Trans.* **1965**, *5*, 1.
(26) Fujita, H.; Kishimoto, A. *J. Polym. Sci.* **1958**, *28*, 547.
(27) Ferry, J. D. *Viscoelastic Properties of Polymers*; Wiley: New York, 1980; p 287.
(28) Reichl, L. E. *A Modern Course in Statistical Physics*; University of Texas Press: Austin, 1980; p 167.